Cement and Concrete Research 40 (2010) 892–897

Contents lists available at ScienceDirect

Cement and Concrete Research

journal homepage: http://ees.elsevier.com/CEMCON/default.asp

The structure of alkali silicate gel by total scattering methods

C.J. Benmore [a], Paulo J.M. Monteiro [b,*]

[a] Argonne National Laboratory, 9700 S. Cass Avenue, Argonne, IL 60439, USA
[b] Department of Civil and Environmental Engineering, University of California at Berkeley, CA 94720, USA

ARTICLE INFO

Article history:
Received 2 December 2008
Accepted 15 February 2010

Keywords:
Alkali–aggregate reaction (C)
Amorphous material (B)
Deterioration (C)
Pair distribution function
Total scattering
X-ray (B)

ABSTRACT

The structure of the alkali silicate gel (ASR) collected from the galleries of Furnas Dam in Brazil was determined by a pair distribution function (PDF) analysis of high energy X-ray diffraction data. Since this method is relatively new to concrete structure analysis a detailed introduction on the PDF method is given for glassy SiO_2. The bulk amorphous structure of the dam material is confirmed as no Bragg peaks are observed in the scattered intensity. The real space results show that the local structure of the amorphous material is similar to kanemite ($KHSi_2O_5{:}3H_2O$) however the long range layer structure of the crystal is broken up in the amorphous state, so that ordering only persists of the length scale of a few polyhedra. The silicate layer structure is a much more disordered than predicted by molecular dynamics models. The X-ray results are consistent with the molecular dynamics model of Kirkpatrick et al. (2005) [1] which predicts that most of the water resides in pores within the amorphous network rather than in layers. The total scattering data provide a rigorous basis against which other models may also be tested.

1. Introduction

For concrete structures, the alkali silicate reaction is a serious deleterious interaction that occurs between reactive aggregates containing amorphous or poorly crystalline silica with alkali and hydroxide ions in the concrete pore solution. The reaction generates an amorphous gel that, by adsorbing large amounts of water, expands and if confined in the matrix can generate large enough stresses that can crack the concrete. There are many classical methods to prevent the reaction such as the use of fly ash [2,3], silica fume [4], slag [5,6], natural pozzolans [7], lithium [8], bricks [9] and microfibers [10] but the repair methods for damaged structures are still at its infancy. Therefore there is a great interest in characterizing the structure of the gel to optimize the concrete mixture and to develop improved repair methods. NMR results suggest that the ASR gel is an amorphous alkali (sodium or potassium)-hydroxide-silicate glass with a Q^3-speciation dominant connectivity [11]. Tambeli et al. [12] reported that the number of mean number of non-bridging oxygens for the ASR gel was around 1.0 much higher than the value of 0.51 for potassium-silicate glasses with the same K_2O content, indicating the presence of a substantial number of hydroxyl groups contributing to depolymerisation of the ASR gel. The model proposed by Wieker [13–15] that the ASR gel has a structure similar to Na or K silicate kanemite [$(Na,K)HSi_2O_5{:}3H_2O$] has been gaining acceptance. Kanemite has a layered structure of corrugated $[Si_2O_4OH]_n$ sheets and hydrated Na (or K) [16–18]. The alkali cations are coordinated to six water molecules, developing layers of distorted octahedra.

Kirpatrick et al. [1] performed an insightful molecular dynamics (MD) model for kanemite and ASR gel. Their result indicates that the amount of water capable of entering the interlayer spaces of kanemite is limited so they proposed that expansion of the ASR gel is caused mainly by the adsorption of water between nanoparticles. The determination of the gel structure and location of water in the gel is fundamental for the understanding of the ASR reaction and for the development of remedial actions for the damaged concrete structures. The purpose of this paper is to take advantage of recent progress obtained in the characterization of glasses using high energy X-ray total scattering methods to analyze the ASR gel. This powerful characterization method, including the pair distribution function, can be used to study any amorphous or poorly crystalline phases in concrete (vitreous phases in mineral admixtures, amorphous silica in the aggregate, calcium silicate hydrates, among others) so we will include a brief introduction of the methodology.

Radial distribution function methods (now often referred to as pair distribution function or total scattering methods) have been used since the 1930s [19], mainly through the X-ray and neutron investigations into the disordered structure inherent in liquids and amorphous materials [20,21]. The experimental set up essentially comprises of a collimated, monochromatic radiation beam impinging on a sample and scattering through an angle into a position sensitive detector [22]. Two modern variations of this technique for studying disorder in materials with high local structural resolution, are time of flight neutron diffraction and high energy X-ray diffraction [23]. Both techniques exploit the availability of high flux, low wavelength

* Corresponding author.
E-mail address: monteiro@ce.berkeley.edu (P.J.M. Monteiro).

0008-8846/$ – see front matter © 2010 Published by Elsevier Ltd.
doi:10.1016/j.cemconres.2010.02.006

sources and small scattering angles to minimize complex attenuation and multiple scattering corrections to the data. The pair distribution function (PDF) method involves the Sine Fourier transform of the measured structure factor over a wide momentum transfer range, providing a direct measure of the probability, $G(r)$, of finding an atom surrounding a central atom at a radial distance away, r [24]. The weighting factor of each atomic species is being scaled by their concentration and by the number of electrons for X-rays or coherent neutron scattering length for neutrons. The advantage is that average structural information may be obtained when no Bragg peaks are present in the measured diffraction pattern and all the scattering data is taken into account, hence the name total scattering.

2. Methods

2.1. Total scattering

To illustrate the sensitivity of different diffraction probes the X-ray and neutron structure factors for amorphous SiO_2 are compared directly in Fig. 1 using data from Mei et al. [25]. The most noticeable difference is the appearance of the Q_2 peak in the neutron spectrum. To understand this we consider that the X-ray weighted total structure factor can be written in terms of the sum of several real space probability functions [26,27],

$$S_X(Q)-1 = \sum_{i,j=1}^{n} c_i c_j f_{ij}(Q)\left[S_{ij}(Q)-1\right] \quad (1)$$

$$= \rho_o \sum_{i=1}^{n} c_i c_j f_{ij}(Q) \int_0^{\infty} 4\pi r^2 \left[g_{ij}(r)-1\right]\frac{\sin Qr}{Qr} dr$$

where $\rho_o = N/V$ is the atomic number density (in atoms/Å^3), c_i is the atomic concentration of atoms of species i, $S_{ij}(Q)$ are the partial structure factors, $g_{ij}(r)$ are the corresponding partial pair distribution functions, Q is the scattering vector, r is the distance in real space and

$$f_{ij}(Q) = \frac{f_i(Q)f_j(Q)}{\left[\sum_{i=1}^{n} c_i f_i^2(Q)\right]}. \quad (2)$$

$f_i(Q)$ is the X-ray (usually atomic) form factor for species i. We note that the neutron case has a similar representation whereby $f_i(Q)$ is replaced by the coherent neutron scattering length b_i. We note that hydrogen is often replaced with deuterium in neutron experiments due to complex recoil effects, which make data reduction difficult for samples containing high (>10%) hydrogen contents [28]. However, we include the technique here in the case of SiO_2 to illustrate the complimentarity of the PDF neutron and X-ray techniques.

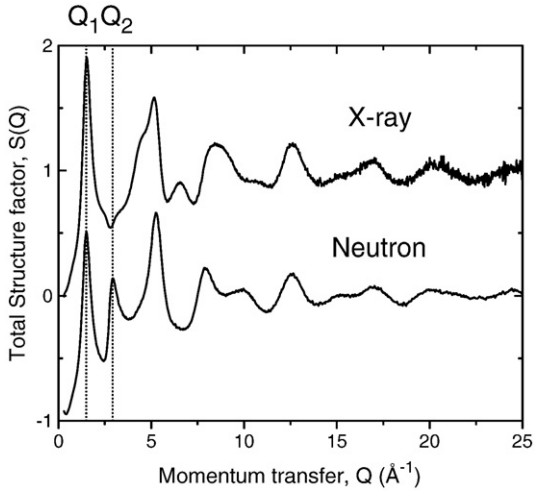

Fig. 1. Measured X-ray and neutron total structure factors for vitreous SiO_2 as a function of momentum transfer in inverse Angstrom (Å). Q_1 and Q_2 mark the positions of the first and second diffraction peaks.

For a system containing N species or atom types, there are $N(N+1)/2$ partial structure factors $S_{ij}(Q)$. If we take glassy SiO_2 as an example, $N=2$ and there are three partial structure factors, namely $S_{SiSi}(Q)$, $S_{SiO}(Q)$ and $S_{OO}(Q)$ [29]. Writing the X-ray case of Eq. (1) for SiO_2 we have,

$$S_X(Q)-1 = \frac{c_{Si}^2 f_{Si}^2(Q)[S_{SiSi}(Q)-1] + 2c_{Si}c_O f_{Si}(Q)f_O(Q)[S_{SiO}(Q)-1] + c_O^2 f_O^2(Q)[S_{OO}(Q)-1]}{c_{Si}^2 f_{Si}^2(Q) + 2c_{Si}c_O f_{Si}(Q)f_O(Q) + c_O^2 f_O^2(Q)}. \quad (3)$$

Given that the atomic concentrations of Si and O are $c_{Si}=1/3$ and $c_O=2/3$ respectively, and that the number of electrons are $f_{Si}=14$ and $f_O=8$, at $Q=0$ Å^{-1} Eq. (3) reduces to,

$$S_X(Q=0)-1 = 0.218[S_{SiSi}(0)-1] + 0.498[Si_{SiO}(0)-1] + 0.284[S_{OO}(0)-1]. \quad (4)$$

A similar expression can be obtained for neutrons,

$$S_N(Q)-1 = 0.069[S_{SiSi}(Q)-1] + 0.388[Si_{SiO}(Q)-1] + 0.543[S_{OO}(Q)-1]. \quad (5)$$

The X-ray spectrum is most highly weighted by the Si–O interactions, in contrast the neutron spectra are heavily weighted towards the oxygen interactions. The Q_2 peak in the neutron spectrum arises from O–O interactions.

2.2. Intermediate range order in an amorphous material

A schematic 2D model glass structure illustrating the origin of the Q_1 and Q_2 peaks in $S_X(Q)$ and $S_N(Q)$ for SiO_2 is also shown in Fig. 2. The addition of alkali ions into the silicate matrix effectively breaks up the SiO_2 cage network [30], and as a consequence the height of the Q_1 decreases with alkali content. Pure glassy SiO_2 comprises of a fully polymerized network in which each oxygen bridges i.e. only Q^4 speciation. Furthermore, the first sharp diffraction peak, Q_1, in Fig. 1 has been associated with intermediate range ordering, referring to ordering beyond the first few nearest neighbour tetrahedra, which occur with a periodicity of $2\pi/Q_1 \sim 6$ Å arising from cages in the network [22]. For a layered silicate such as kanemite [15], Q_1 is associated with the layering of sheets in a 2D network with mainly Q^3 speciation. The second diffraction peak at position Q_2 has been associated with chemical ordering of like atoms with a periodicity of $2\pi/Q_2 \sim 3$ Å [31], which can also extend to distances >5 Å. The similar features at high momentum transfer, beyond $Q>7.5$ Å^{-1}, arise from the detailed structure of the average local structural units, in Fig. 1 this relates to SiO_4 tetrahedra. Wright [21] has rationalized the ordering in single component network glasses on both of these length scales, as being consistent with Zachariasen's 'random' network theory of glasses [32] (illustrated in Fig. 2), where the extent of intermediate range ordering is defined by 'the limit of distortion of the local structural unit and the allowed distribution of bond torsion angles'.

2.3. Pair distribution functions

The Sine Fourier transform of the structure factor $S_X(Q)$ can be defined as the total X-ray pair distribution function $G_X(r)$ through [24],

$$G_X(r) = \frac{f_i(Q)f_j(Q)}{(2\pi)^3\rho_o}\int_0^{\infty} 4\pi Q^2 S_X(Q)\frac{\sin Qr}{Qr} dQ. \quad (6)$$

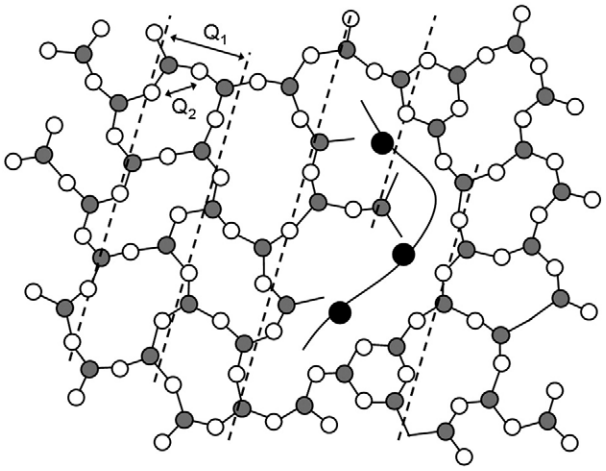

Fig. 2. Zachariasen [32] – Wright [21] network model of a glass in which the structure is random within the steric packing constraints of the local unit(s). The dashed lines of periodicity Q_1 arise from correlations between cages which comprise the glassy silicate network. Q_2 represents the length scale of the bulk chemical ordering of the network. The black circles represent the modifier atoms which break up the connectivity of the silicate network.

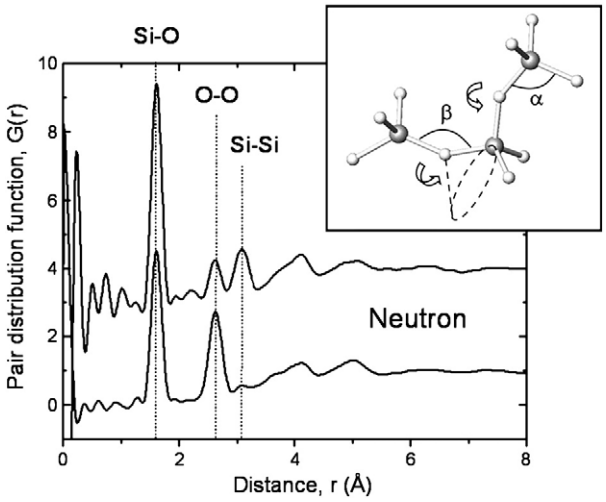

Fig. 3. The total X-ray and neutron radial pair distribution functions for vitreous SiO_2. The curves were obtained from a direct Sine Fourier transformation of the measured structure factors shown in this figure. The inset shows the local tetrahedral and packing torsion angles.

$G_X(r)$ emphasizes the local structural correlations and is commonly used in the studies of liquids and computed in Molecular Dynamics or Monte Carlo simulations.

It is sometimes useful to define the differential distribution function $D_X(r)$ [29],

$$D_X(r) = 4\pi r\rho_o[G_X(r)-1]. \quad (7)$$

$D_X(r)$ has the advantage that the bulk density has been removed, highlighting small structural changes at higher-r values, and is most convenient for plotting because it makes best use of the plotting area. Also,

$$N_X(r) = 4\pi r^2\rho_o G_X(r) \quad (8)$$

has a direct physical interpretation, since $N(r)\mathrm{d}(r)$ represents the number of atoms lying within a range $(r, r+\mathrm{d}r)$ from any given atom.

For our example of glassy SiO_2 we take the Fourier transforms of curves represented by Eqs. (4) and (5) to obtain the corresponding X-ray $G_X(r)$ and neutron $G_N(r)$ pair distribution functions which are shown in Fig. 3. Note the relative sizes of the first three peaks in the neutron and the X-ray case and their correlation with the element specific weighting factors in Eqs. (4) and (5). This is more clearly explained in Fig. 4 which shows the breakdown of the total pair distribution function, $G_X(r)$, for glassy SiO_2 in terms of its three partial structure factors, $g_{ij}(r)$, and how specific atomic correlations between adjacent tetrahedra contribute in each case.

The general structural characteristics of a PDF measurement on an amorphous material fall into three main categories [22]:

(i) Local structural unit(s). These polyhedra are usually defined by the first few peaks in the pair distribution function i.e. the tetrahedral unit in vitreous SiO_2. The peaks corresponding the Si–O bond, the O–O distance that defines the local SiO_4 unit with an angle of $\alpha = 109.5°$ for a perfect tetrahedra are shown in the insert of Fig. 3. Since these correlations are at the shortest distances in real space they correspond to the oscillations at the higher-Q values in reciprocal space.

(ii) Polyhedral connectivity. Average orientations of adjacent polyhedra are defined by distances typically up to 5 or 6 Å depending on their size. Although much longer 'extended range' correlations, due to the chemical ordering of atoms, have also been reported. In our example of vitreous SiO_2 the periodicity of the Si–Si and O–O correlations is largely associated with the second sharp diffraction peak, Q_2 in reciprocal space (see Fig. 1). Information in this region of the real space pair distribution functions defines the range of bond torsion angles within the material. For glassy SiO_2 the Si–Si peak position gives an average Si–O–Si torsion angle of $\beta = 146°$ which indicates the corner shared connectivity of the tetrahedra and correlates with rather open network in vitreous SiO_2 associated primarily with 5, 6 and 7-membered rings.

(iii) Intermediate range order. This is typically 5–20 Å and arises from the distribution of different sized cages in a 3D network like vitreous SiO_2 [25], layers in a 2D material such as a clay or chains in a 1D system. Intermediate range order is usually associated with repeated atomic correlations across open void spaces between groups of atoms in a network glass (see Fig. 2) and is most readily associated with the first sharp diffraction peak at position Q_1 in the measured structure factor as discussed earlier. The position and shape of the FSDP are sensitive to the distribution of different sized ring or cage structures within the material.

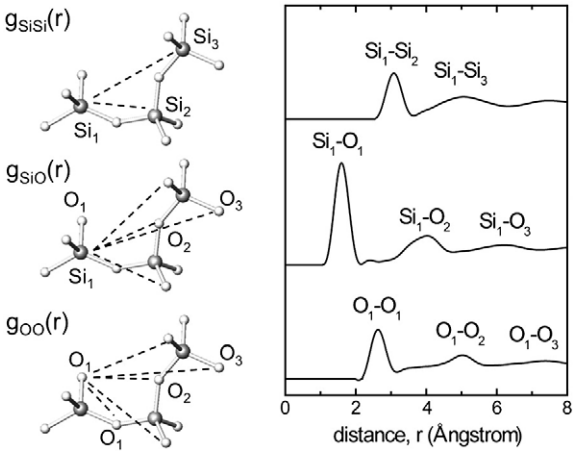

Fig. 4. The three atom specific partial pair distribution functions for vitreous SiO_2; $g_{SiSi}(r)$, $g_{SiO}(r)$ and $g_{OO}(r)$ taken from Ref. [29]. The peaks in the distribution functions are illustrated by the distances indicated in the atomistic plots of three corner shared SiO_4 tetrahedra. Faber and Ziman [26] defined partial pair distribution functions in terms of element specific contributions. For SiO_2 there are three partials, namely Si–O, O–O and Si–O. For a more complex system containing N atom types there are $N(N+1)/2$ partial structure factors.

2.4. Application to the alkali silicate gel

Given these considerations, we apply the X-ray PDF technique previously described for amorphous SiO_2, to a more complex amorphous sample K-kanemite, $KHSi_2O_5{:}3H_2O$. Here $N=4$, so there are ten partial distribution functions contributing to the measured total $G_X(r)$ and many peaks will overlap making it impossible to isolate most of the atom–atom correlations. Nonetheless, using chemical knowledge of common bond lengths, comparing with known crystal structures and making direct comparisons with molecular dynamics simulations it is possible to build up a picture of a realistic atomic model consistent with the total scattering data.

3. Experimental procedure

3.1. Collection of the gel

Furnas Dam used reactive quartzite rock as the aggregate for concrete and, over of time, cracks caused by alkali silica reaction were formed. Structural repairs were successfully performed and the dam has been generating energy without interruption. The deleterious reaction starts with the dissolution of the aggregates and formation of the gel near the aggregate but over time as the reaction continues the gel can migrate through the porous matrix and can create macroscopic clusters, in the order of cm, on the surface of the damaged structure. Exuded gels were observed along the drainage gallery of the dam and these gels were collected for chemical and structural analysis. The measured average K/Si atomic ratio of the gel was 0.37 and the samples were finely ground for the X-ray diffraction experiments. NMR analysis of the gel can be found in [11,12].

3.2. Testing methods

When hard X-rays (Energy, $E>50$ keV) are used, it is possible to measure $S_X(Q)$ to much higher momentum transfers thereby increasing local real space resolution [33]. In addition, problematic attenuation and multiple scattering effects are negligible for small samples (~1 mm^3) [33]. This is because the photo-electrical absorption decreases as $\sim E^{-3}$ and scattering typically becomes the dominant process, under conditions similar to that of a neutron diffraction experiment. In this experiment high energy X-ray diffraction measurements were conducted on beamline 1-ID at the Advanced Photon Source, Argonne National Laboratory, using an incident beam energy of 100.0 keV and a two-dimensional GE amorphous silicon area detector [34]. The momentum transfer scale was calibrated by refining a standard crystalline CeO_2 sample using the program *FIT2D* [35]. The background was removed from the integrated sample data and normalized at high-Q values to the 'self' scattering calculated from the tabulated atomic form factors of Hubbell [36] plus the Compton scattering (see Fig. 5) using the relation,

$$S_X(Q)-1=\frac{I_X(Q)-C(Q)-\sum_{i=1}^{n} c_i f_i^2}{\left[\sum_{i=1}^{n} c_i f_i(Q)\right]^2}. \quad (10)$$

This gave a reliable total structure factor, $S_X(Q)$, for amorphous K-kanemite up to $Q\sim 30$ Å^{-1} indicating that all the necessary corrections had been applied and the composition $KHSi_2O_5{:}3H_2O$ is correct (see Fig. 5). The results show a small peak at $Q_1=0.65$ Å^{-1}, corresponding to a periodicity of 9.7 Å within the amorphous structure (see insert of Fig. 6) and a much larger, second peak at $Q_2=1.85$ Å^{-1}. The $S_X(Q)$ curve was Fourier transformed using Eq. (1)

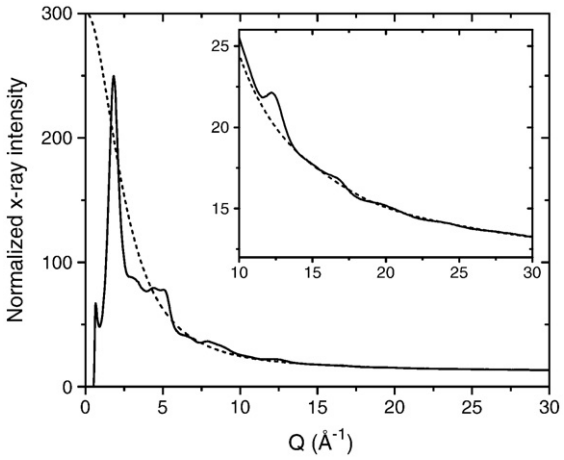

Fig. 5. The measured and background corrected X-ray intensity for the amorphous K-kanemite gel ($KHSi_2O_5{:}3H_2O$, solid line) normalized to the sum of the constituent atomic form factors squared (the self scattering) plus the Compton scattering (dashed line) at high Q.

with a Lorch modification function [37] to suppress any artifacts from the finite measured Q-range as described by Wright [22].

4. Results

The X-ray total pair distribution function, $G_X(r)$ is shown in Fig. 7 (a). Bond length and local structural correlations for amorphous K-kanemite can be made on three counts (i) the basis of chemical knowledge (ii) comparison with the crystal structure K-kanemite and (iii) by comparing to existing molecular dynamics simulations on Na-kanemite. Bond valence theory and crystallographic bond distances for varying size polyhedra have been detailed by Shannon and Prewitt [38]. For example, a Si–O distance of ~1.64 Å is indicative of SiO_4 tetrahedra, whereas a K–O distance of ~2.78 Å would be indicative of KO_6 octahedra. The peaks at 1.62 Å and 2.66 Å (O–O) in the measured spectra are therefore assigned to the existence of SiO_4 tetrahedra. Assignment of peaks at higher-r is difficult due to peak overlap. The KO_6 peak is most likely hidden under the O–O peak in our experiment, but based on comparison with the MD model for the Na-kanemite gel [1], see Fig. 7(b). We attribute the following peaks in $G_X(r)$ to the dominant correlations: 3.08 Å (Si–Si), followed by a low-r shoulder at 3.8 Å (Si–O_2) on a larger peak at 4.13 Å (K–O). These are illustrated in more detail in Fig. 8. The higher-r peaks have multiple contributions 4.97 Å (O–O/Si and Si–Si/K), 6.40 Å (O–O/Si/K) and 7.43 Å (Si–Si, O–O, and K–Si).

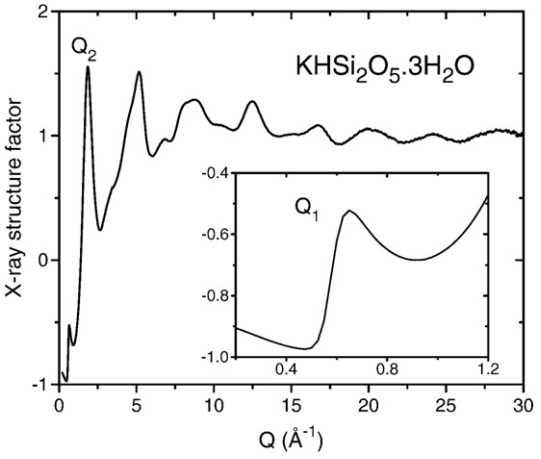

Fig. 6. The measured total X-ray structure factor for the amorphous K-kanemite gel.

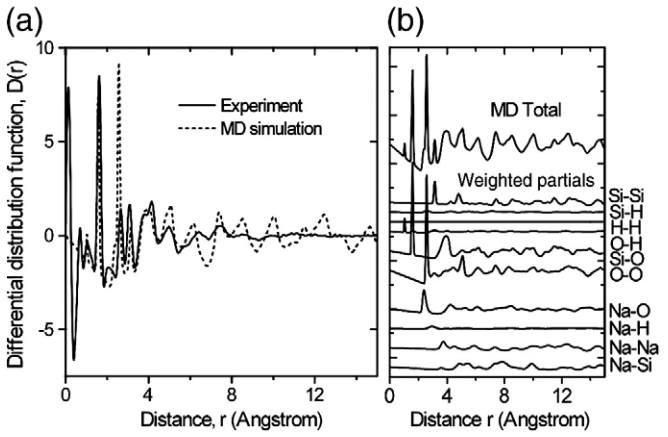

Fig. 7. (a) The measured X-ray pair distribution function for amorphous K-kanemite gel (solid line, this study) compared to that predicted by molecular dynamics (MD) simulation for amorphous Na-kanemite ($NaHSi_2O_5{:}3H_2O$, Kirkpatrick et al. [1], dashed line). (b) The atom specific weighted partial structure factors from the MD simulation and the predicted total X-ray distribution function.

5. Discussion

The alkali silicate reaction (ASR) in concrete occurs to produce a hydrous gel which can swell by incorporating large amounts of water causing severe and irreversible expansion and cracking. Wieker et al. [13–15] have proposed that ASR gel has a similar structure to the layered structure of crystalline hydrous kanemite. The crystal structure of kanemite consists of sheets of corrugated SiO_4 tetrahedra and hydrated K atoms [16–18]. The silicate sheets contain six membered rings of Q^3 units, where three bridging oxygens are corner shared with other SiO_4 tetrahedra and the non-bridging oxygen points to the interlayer region. The K atoms coordinate to six water molecules, forming interlayer chains of distorted edge shared octahedra, which are corner shared to adjacent chains. The interlayer spacing between the corrugated SiO_4 sheets is ~10 Å.

X-ray diffraction experiments have confirmed the amorphous nature of K silicate field gels, exhibiting a broad principal peak at $Q_2 \sim 1.9$ Å^{-1} and a smaller low-Q peak at $Q_1 = 0.6$ Å^{-1} which moves to lower Q values (longer distances) when hydrated [11]. The gels containing K are being somewhat more disordered than those gels containing Na. The relatively low intensity of the first peak in our K-gel data at $Q_1 = 0.65$ Å^{-1}, compared to that of pure SiO_2 in Fig. 1, suggests the ordering of sheets does not persist much beyond a few layers in real space [20,29]. ^{29}Si MAS NMR measurements for these have shown the gels retain high concentrations of SiO_4 tetrahedra with Q^3 polymerization together with some Q^4, Q^2 and Q^1 sites. About 50% of the non bridging oxygens in ASR gel from in-service concrete are occupied by H^+ (Si–OH groups) and 50% are charge balanced by the alkali cations.

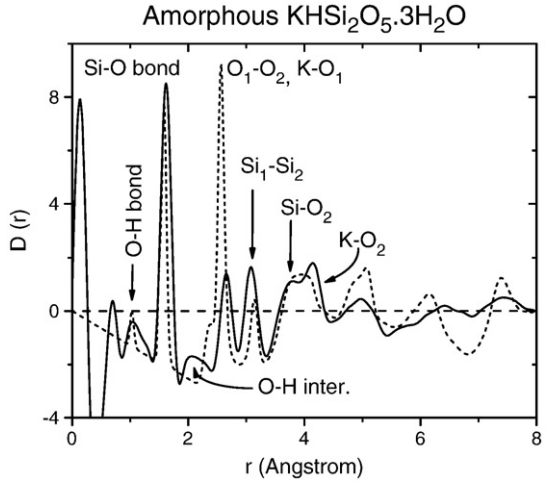

Fig. 8. The X-ray differential distribution function $D(r)$ for the amorphous K-kanemite gel ($KHSi_2O_5{:}3H_2O$, solid line) compared to the MD Na-Kanemite model (dashed line [1]). Peak assignment comprising the local polyhedra and connectivity of these units is based on the model shown in Fig. 9 [11].

Molecular dynamics simulations have been carried out by Kirkpatrick et al. [1] on crystalline Na-kanemtite to try and address the structural mechanisms by which it incorporates water. Possible scenarios put forward included the addition of water molecules between the layers, a de-polymerization of the silicate layers themselves or interstitial water regions between nanoparticles of kanemite. The molecular dynamics simulations predicted that the alkali silicate layer structure is held together quite strongly and the water molecules are incorporated between kanemite particles rather than being able to penetrate within the layers or between the interlayer regions.

A direct comparison of our measured differential distribution function on K-kanemite is compared to the same function calculated from the published molecular dynamics simulation data of Kirkpatrick et al. [1] performed on Na-kanemite and shown in Fig. 7(b). The most apparent difference is that the first nearest neighbour oxygen–oxygen distances within the SiO_4 tetrahredra. We note that the oxygen–oxygen peak from SiO_4 tetrahedra dominates the X-ray signal at this distance and substantial differences between the experiment and simulation in this region can only be accounted for by significant changes to the O–O peak. This indicates that the silica tetrahedra are considerably more distorted than the molecular dynamics model predicts (the experimental peak is much smaller and broader) leading to a more 'random' network structure beyond the distance of a few interconnected polyhedra, rather than a well defined nano-crystalline layered structure. The bulk gel structure of the material we studied was not crystalline as no Bragg peaks are observed in the scattered intensity. Otherwise the agreement up to $r = 4.5$ Å between the Na-kanemite MD model [1] with experiment is reasonably good, despite the difference in cation. For the 5 Å peak and beyond the measured peaks are notably smaller in the experimental gel spectra, compared to the crystalline Na-kanemite simulation model and no distinct structural correlations are observed beyond ~10 Å i.e. ordering only persists the length scale of four or five polyhedra. Fig. 7 shows that the 5 Å peak has two contributions; the Si_1–Si_3 at 4.8 Å and the O_1–O_2 at 5.08 Å. This implies that the average orientations of the second and third nearest neighbour SiO_4 tetrahedra are much more disordered than those in the regularly aligned corrugated crystalline sheets, which may allow some water molecules to penetrate the silicate layers.

The MD simulation results [1] suggest that it is energetically unfavourable for the water to penetrate the interlayer volume in significant quantity and that for the large expansions observed in the gel, a continuous polymerized silicate layer is in any case unlikely. The PDF measurements are consistent with this scenario. The persistence of a distorted kanemite-like structure is in good agreement with the MD simulation, however the PDF data also indicate that a refinement of this model is needed. A revised structural model of $KHSi_2O_5{:}3H_2O$ gel involves small clusters of K-octahedra surrounded by distorted silicate layers, which show no distinct preferred orientational correlations beyond ~10 Å. Due to the lack of long range ordering in this material we suggest that water molecules probably reside in pores surrounding these kanemite-like fragments as well as within the layers themselves. A schematic atomic arrangement of such a structure consistent with the diffraction data is shown in Fig. 9. Here the water molecules are depicted attaching to the surfaces of the silicate layers and K-ion clusters [39].

6. Conclusions

The agreement between the experimental PDF and the MD simulation in the region 3–5 Å in Fig. 6 indicates that fragments of the silicate network are still intact, albeit with a larger degree of

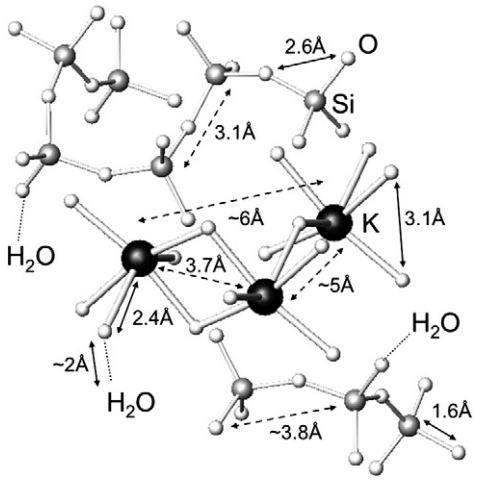

Fig. 9. A local structural model of the amorphous K-kanemite ($KHSi_2O_5{:}3H_2O$) gel consistent with the diffraction data by comparison to the ideal K-kanemite crystal structure [11].

orientational freedom than predicted. In particular the 3.1 Å peak indicates a well defined connectivity between adjacent Si–Si tetrahedral, as illustrated in Fig. 3 for pure glassy SiO_2. In addition, the peak in $S(Q)$ at Q_1 suggests that these fragments are arranged in layers within the ASR gel, with a periodicity of 9.7 Å. We therefore conclude that, in line with the model suggested by Kirkpatrick et al., a local K-kanemite-like structure persists in the gel and the water probably most likely resides in pores around these layered regions, but some water may also penetrate within and between the layers themselves. The water most likely attaches to non-bridging oxygens in the interfacial regions bounded by a distorted silicate layers and to small clusters of K-octahedra (see model in Fig. 9). More measurements are needed to see how the local kanemite structure changes with increasing water content and the gel expands.

X-ray PDF provides a rigorous test of MD simulation models, and clearly highlights any inadequacies in the proposed structure. It is anticipated that a comparison of MD inter-atomic potentials with the partial PDFs of pure glassy SiO_2, will prove useful for molecular dynamics simulators in developing more realistic inter-atomic potentials, which may be used to predict the structure of more complex systems such as K-kanemite gel. In addition, the approach of combining PDF with other techniques, such as NMR for example e.g. [40], will hopefully lead to the development of more accurate 3D structural models of cement.

Acknowledgements

This work was supported by the U.S. DOE, Argonne National Laboratory under contract number DE-AC02-06CH11357. This publication was based on work supported in part by Award No. KUS-I1-004021, made by King Abdullah University of Science and Technology (KAUST) and by the National Science Foundation grant 062464. R.J. Kirkpatrick is thanked for providing the molecular dynamics simulation data.

References

[1] R.J. Kirkpatrick, A.J. Kalinichev, X. Hou, L. Struble, Mater. Struct. 38 (2005) 449.
[2] P.K. Mehta, P.J.M. Monteiro, Concrete, Structure, Properties, and Materials, 3rd ed. McGraw-Hill, 2006.
[3] Benoit Fournier, Marc-André Bérubé, Alkali–aggregate reaction in concrete: a review of basic concepts and engineering implications, Can. J. Civ. Eng. 27 (2) (2000) 167–191.
[4] N.P. Hasparyk, P.J.M. Monteiro, H. Carasek, Effect of silica fume and rice husk ash on the alkali–silica reaction, ACI Mater. J. 97 (4) (2000) 486–492.
[5] M. Prezzi, P.J.M. Monteiro, G. Sposito, Alkali–silica reaction — part 2: the effect of chemical additives, ACI J. 95 (1998) 3–10.
[6] P.J.M. Monteiro, K. Wang, G. Sposito, M.C. dos Santos, W. Pacelli de Andrade, Influence of mineral admixtures on the alkali–aggregate reaction, Cem. Concr. Res. 27 (1997) 1899.
[7] D.W. Hobbs, Alkali–silica Reaction in Concrete, American Society of Civil Engineers, 1988.
[8] J.F. Schneider, N.P. Hasparyk, D.A. Silva, P.J.M. Monteiro, Effect of lithium nitrate on the ASR gel, Am. Ceram. Soc. 91 (10) (2008) 3370–3374 Published: OCT 2008.
[9] L. Turanli, F. Bektas, P.J.M. Monteiro, Use of ground clay brick as a pozzolanic material to reduce the alkali–silica reaction, Cem. Concr. Res. 33 (10) (2003) 1539–1542.
[10] L. Turanli, K. Shomglin, C.P. Ostertag, P.J.M. Monteiro, Reduction in alkali–silica expansion due to steel microfibers, Cem. Concr. Res. 31 (2001) 825–827.
[11] X. Hou, L.J. Struble, P.J.M. Monteiro, R. James Kirkpatrick, Structural investigations of alkali silicate gels, J. Am. Ceram. Soc. 88 (4) (2005) 943–949.
[12] C.E. Tambelli, J.F. Schneider, N.P. Hasparyk, P.J.M. Monteiro, Study of the structure of alkali–silica reaction gel by high-resolution NMR spectroscopy, J. Non-Cryst. Solids 352 (2006) 3429–3436.
[13] W. Wieker, C. Hubert, D. Deidemann, Recent results of solid-state, NMR investigations and their possibilities of use in cement chemistry, Proceedings of the 10th International Congress on Chemistry of Cements, 1997, pp. 395–408.
[14] W. Wieker, C. Hubert, D. Heidemann, R. Ebert, Alkali–silica reaction — a problem of the insufficient fundamental knowledge of its chemical base, Mater. Sci. Concrete, Spec. Vol. (Sidney Diamond Symposium) (1998) 395–408.
[15] W. Wieker, C. Hubert, D. Heidemann, R. Ebert, Some experiences in chemical modelling of the alkali–silica reaction, 11th International Conference on Alkali–Aggregate Reaction, 2000, pp. 119–128.
[16] C. Apperley, M.J. Hudson, M.T.J. Keene, J.A. Knowles, Kanemite ($NaHSi_2O_5{\cdot}3H_2O$) and its hydrogen-exchanged form, J. Mater. Chem. 5 (4) (1995) 577–582.
[17] K. Beneke, G. Lagaly, Kanemite-innercrystalline reactivity and relations to other sodium silicates, Am. Mineral. 62 (7–8) (1977) 763–771.
[18] A.J. Garvie, B. Devouard, T.L. Groy, F. Camara, P.R. Buseck, Crystal structure of kanemite, $NaHSi_2O_5{\cdot}3H_2O$, from the Aris phonolite, Namibia, Am. Mineral. 84 (7–8) (1999) 1170–1175.
[19] B.E. Warren, H. Krutter, O. Morningstar, Fourier analysis of X-ray patterns of vitreous SiO_2 and B_2O_3, J. Am. Ceram. Soc. (202) (1936) 202–206.
[20] D.L. Price, S.C. Moss, R. Reijers, M.-L. Saboungi, S. Susman, Intermediate-range order in glasses and liquids, J. Phys. Condens. Mat. 1 (1989) 1005–1008.
[21] A.C. Wright, Neutron scattering from vitreous silica V. The structure of vitreous silica, J. Non-Cryst. Solids 179 (1994) 84–115.
[22] A.C. Wright, Longer range order in single component network glasses, Phys. Chem. Glasses: Eur. J. Sci. Tech. B 49 (2008) 103–117.
[23] P.A. Egelstaff, Introduction to the Liquid State, 2nd EdClarendon Press, Oxford, 1992 p15.
[24] M.C. Wilding, C.J. Benmore, Structure of glasses and melts in neutron scattering in earth sciences, chapter 12, Rev. Mineral. Geochem. 63 (2006) 275–311.
[25] Q. Mei, C.J. Benmore, S. Sen, R. Sharma, J.L. Yarger, Intermediate range order in vitreous silica from a partial structure factor analysis, Phys. Rev. B 78 (2008) 144204.
[26] T.E. Faber, J.M. Ziman, A theory of the electrical properties of liquid metals, Phil. Mag. 11 (1965) 153.
[27] D.A. Keen, A comparison of various commonly used correlation functions for describing total scattering, J. Appl. Cryst. 34 (2001) 172–177.
[28] J.C. Dore, M. Garawi, M.C. Bellisent-Funel, Neutron diffraction studies of the structure of water at ambient temperatures, revisited [a review of past developments and current problems], Mol. Phys. 102 (2004) 2015–2035.
[29] S. Susman, K.J. Volin, D.G. Montague, D.L. Price, The structure of vitreous and liquid GeSe2: a neutron diffraction study, J. Non-Cryst. Solids 125 (1990) 168–180.
[30] G.N. Greaves, A. Fontaine, P. Lagarde, D. Raoux, S.J. Gurman, Local structure of silicate glasses, Nature 293 (1981) 611–616.
[31] P.S. Salmon, R.A. Martin, P.E. Mason, G.J. Cuello, Topological versus chemical ordering in network glasses at intermediate and extended lengthscales, Nature 435 (2005) 75–78.
[32] W.H. Zachariasen, The atomic arrangements in glass, J. Am. Chem. Soc. 54 (1932) 3841–3851.
[33] H.F. Poulsen, J. Neuefeind, H.B. Neumann, J.R. Schneider, M.D. Zeidler, Amorphous silica studied by high energy X-ray diffraction, J. Non-Cryst. Solids 188 (1995) 63–74.
[34] Q. Mei, C.J. Benmore, R.T. Hart, E. Bychkov, P.S. Salmon, C.D. Martin, F.M. Michel, S.M. Antao, P.J. Chupas, P.L. Lee, S.D. Shastri, J.B. Parise, K. Leinenweber, S. Amin, J.L. Yarger, Topological changes in glassy GeSe2 at pressures up to 9.3 GPa determined by high energy X-ray and neutron diffraction measurements, Phys. Rev. B. 74 (2006) 014203.
[35] A.P. Hammersley, FIT2D. Internal Report ESRF98HA01T, European Synchrotron Radiation Facility, Grenoble, France, 1998.
[36] J.H. Hubbell, W.J. Veigele, E.A. Briggs, R.T. Brown, D.T. Cromer, R.J. Howerton, Atomic form factors, incoherent scattering functions, and photon scattering cross sections, J. Phys. Chem. Ref. Data 4 (1975) 471.
[37] E. Lorch, Neutron diffraction by germania, silica and radiation-damaged silica glasses, J. Phys. C. Solid State Phys 2 (1969) 229.
[38] R.D. Shannon, C.T. Prewitt, Effective ionic radii in oxides and fluorides, Acta Cryst. B25 (1969) 925–946.
[39] J.A. Allen, J.J. Thomas, H.M. Jennings, Composition and density of nanoscale calcium-silicate-hydrate, Nature Materials 6 (2007) 311–316.
[40] J.C. McLaughlin, S.L. Tagg, J.W. Zwanziger, D.R. Haeffner, S.D. Shastri, J. Non-Cryst. Solids 274 (2000) 1.